

# High-pressure crystal structures and superconductivity of Stannane (SnH<sub>4</sub>)

Guoying Gao<sup>a</sup>, Artem R. Oganov<sup>b,c</sup>, Peifang Li<sup>a</sup>, Zhenwei Li<sup>a</sup>, Hui Wang<sup>a</sup>, Tian Cui<sup>a</sup>, Yanming Ma<sup>a,1</sup>, Aitor Bergara<sup>d,e,f</sup>, Andriy O. Lyakhov<sup>b</sup>, Toshiaki Itaka<sup>g</sup>, and Guangtian Zou<sup>a</sup>

<sup>a</sup>National Laboratory of Superhard Materials, Jilin University, Changchun 130012, P. R. China; <sup>b</sup>Department of Geosciences, Department of Physics and Astronomy, and New York Center for Computational Sciences, Stony Brook University, Stony Brook, NY 11794-2100; <sup>c</sup>Geology Department, Moscow State University, Moscow 119992, Russia; <sup>d</sup>Materia Kondentsatuaren Fisika Saila, Zientzia eta Teknologia Fakultatea, Euskal Herriko Unibertsitatea, 644 Postakutxatila, 48080 Bilbo, Basque Country, Spain; <sup>e</sup>Donostia International Physics Center (DIPC), Paseo de Manuel Lardizabal, 20018, Donostia, Basque Country, Spain; <sup>f</sup>Centro de Física de Materiales Consejo Superior de Investigaciones Científicas Universidad del País Vasco/ Euskal Herriko Unibertsitatea (CSIC-UPV/EHU), 1072 Posta kutxatila, E-20080 Donostia, Basque Country, Spain; and <sup>g</sup>Computational Astrophysics Laboratory, RIKEN, 2-1 Hirosawa, Wako, Saitama 351-0198, Japan

Edited by Russell J. Hemley, Carnegie Institution of Washington, Washington, DC, and approved December 16, 2009 (received for review July 24, 2009)

There is great interest in the exploration of hydrogen-rich compounds upon strong compression where they can become superconductors. Stannane (SnH<sub>4</sub>) has been proposed to be a potential high-temperature superconductor under pressure, but its high-pressure crystal structures, fundamental for the understanding of superconductivity, remain unsolved. Using an *ab initio* evolutionary algorithm for crystal structure prediction, we propose the existence of two unique high-pressure metallic phases having space groups *Ama2* and *P6<sub>3</sub>/mmc*, which both contain hexagonal layers of Sn atoms and semimolecular (perhydride) H<sub>2</sub> units. Enthalpy calculations reveal that the *Ama2* and *P6<sub>3</sub>/mmc* structures are stable at 96–180 GPa and above 180 GPa, respectively, while below 96 GPa SnH<sub>4</sub> is unstable with respect to elemental decomposition. The application of the Allen-Dynes modified McMillan equation reveals high superconducting temperatures of 15–22 K for the *Ama2* phase at 120 GPa and 52–62 K for the *P6<sub>3</sub>/mmc* phase at 200 GPa.

hydrogen-rich compounds | metallization | electron-phonon coupling

Relatively high-temperature superconductivity is now documented in light-element metals such as Li under pressure (1–3) and MgB<sub>2</sub> (4), where transition temperatures  $T_c$  up to 20 K and 39 K, respectively, are observed. There is great interest in exploration of unique superconducting phases in other light-element materials because their high phonon frequencies can enhance electron-phonon coupling (see ref. 5). As the lightest element, hydrogen at very high densities is also predicted to be a superconductor with high transition temperatures (6–8). Experiments indicate that the predicted metallic and superconducting states of hydrogen remain above ~300 GPa (9–11). It has been proposed that hydrogen-rich compounds (e.g., group IVa hydrides (12)) are expected to metallize at pressures considerably lower than pure hydrogen due to the chemical “precompression” caused by heavier elements; these metallization pressures may fall within the range of current capabilities of static compression techniques. The exploration of potential superconductivity in these hydrogen-rich compounds (e.g., SiH<sub>4</sub>, GeH<sub>4</sub>, and SnH<sub>4</sub>) is thus desirable and numerous studies have been performed (13–25). Strikingly, recent experiments (15, 18) show that SiH<sub>4</sub> transforms to a metallic phase near 50–60 GPa with a superconducting  $T_c$  of 17 K at 96 and 120 GPa, though debate remains (26). We have recently predicted (17) that GeH<sub>4</sub> becomes a high-temperature superconductor with a  $T_c$  of 64 K at 220 GPa. A theoretical study of SnH<sub>4</sub> (21) predicts that its  $T_c$  can be even higher, reaching the value of 80 K. Using simulated annealing and geometry optimization, that study found that the high-pressure phase of SnH<sub>4</sub> has *P6/mmm* symmetry with a layered structure intercalated by molecular H<sub>2</sub> units, wherein the nearest H-H distance, 0.84 Å, is short enough to be considered as covalent bonding, but significantly longer than the 0.74 Å in the free H<sub>2</sub> molecule. This prediction of extremely high  $T_c$  is

fully dependent on the correctness of the structural model. Therefore, if some other structures are more stable, the picture of superconductivity in SnH<sub>4</sub> may be completely altered.

Here we undertake a different route to explore the high-pressure structures of SnH<sub>4</sub> and use our newly developed *ab initio* evolutionary simulation method (27–29) to address the above question. This method has proven its reliability and efficiency in predicting stable structures with knowledge only of the chemical composition (17, 30–36). We then performed the calculations on the total energy, band structure, phonons, and electron-phonon coupling of the predicted high-pressure structures. Our results reveal the appearance of unique chemistry of SnH<sub>4</sub> at high-pressure and suggest the high superconductivity of SnH<sub>4</sub> under pressures that are accessible by current experimental technique.

## Results and Discussion

We performed evolutionary variable-cell structure prediction simulations with one to four SnH<sub>4</sub> formula units per cell at 30, 70, 120, 200, and 250 GPa. Analysis of the predicted structures gave us a shortlist of candidate structures with space groups *Cmcm*\* (4 molecules/cell), *P2<sub>1</sub>/m*<sup>†</sup> (2 molecules/cell), *Ama2* (4 molecules/cell) and *P6<sub>3</sub>/mmc* (2 molecules/cell), respectively. In the *Cmcm* and *P2<sub>1</sub>/m* structures predicted at 30 and 70 GPa, the Sn atoms are packed in zigzag chains between which nonbonded H<sub>2</sub> molecules are located. This strongly indicates a tendency to decomposition into Sn + 2H<sub>2</sub>. Indeed, enthalpy calculations (Fig. 2) show that decomposition occurs below 96 GPa.

In the *Ama2* phase, Sn atoms form a simple hexagonal packing, where the trigonal prismatic holes are filled with semimolecular H<sub>2</sub> units (H-H distance 0.79 Å, which is longer than the 0.74 Å in the isolated H<sub>2</sub> molecule). The H<sub>2</sub> units are aligned either along the pseudohexagonal axis, or perpendicular to it, and these two orientations alternate (Fig. 1A). Note that the simple hexagonal structure is a high-pressure form of silicon (*P6/mmm*, ref. (37)), but it is not particularly dense. The *P6<sub>3</sub>/mmc* phase here is based on the much denser hexagonal close packing of the Sn atoms ( $c/a = 1.84$  at 200 GPa, relatively close to the ideal value of

Author contributions: G.G., P.L., Z.L., H.W., and Y.M. performed research; G.G., A.R.O., T.C., Y.M., A.B., A.O.L., T.I., and G.Z. analyzed data; G.G., A.R.O., and Y.M. wrote the paper; and Y.M. designed research.

The authors declare no conflict of interest.

This article is a PNAS Direct Submission.

\*For *Cmcm* structure at 20 GPa, the lattice parameters are  $a = 3.63$  Å,  $b = 9.88$  Å, and  $c = 4.12$  Å with atomic positions of Sn at  $4c$  (0, 0.29142, 0.25) and H at  $4c$  (0, 0.50191, 0.75), (0, 0.42112, 0.75) and  $8f$  (0.96117, 0.49332)

<sup>†</sup>For *P2<sub>1</sub>/m* structure at 70 GPa, the lattice parameters are  $a = 4.89$  Å,  $b = 3.17$  Å,  $c = 3.48$  Å and  $\beta = 89.19^\circ$ , with atomic positions of Sn at  $2e$  (0.64826, 0.25, 0.74596) and H at  $2e$  (0.92488, 0.25, 0.32702), (0.08651, 0.25, 0.38317), (0.02506, 0.25, 0.89266), and (0.18168, 0.25, 0.82398).

<sup>1</sup>To whom correspondence should be addressed. E-mail: mym@jlu.edu.cn.

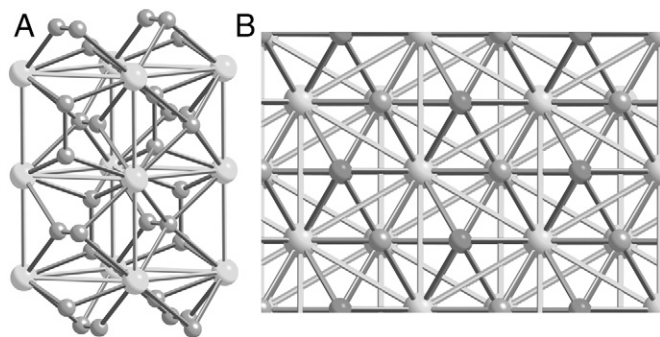


**Fig. 1.** (color online). (A) and (B) *Ama2* and *P6<sub>3</sub>/mmc* structures. For *Ama2* structure at 120 GPa, the lattice parameters are  $a = 5.381 \text{ \AA}$ ,  $b = 5.421 \text{ \AA}$ ,  $c = 3.074 \text{ \AA}$  with atomic positions of Sn at 4a (0, 0, 0.0001) and three inequivalent H atoms at 4b (0.75, 0.58823, 0.00586), 4b (0.75, 0.73278, 0.98835) and 8c (0.87773, 0.32159, 0.99613), For *P6<sub>3</sub>/mmc* structure at 200 GPa the lattice parameters are  $a = b = 2.9024 \text{ \AA}$ ,  $c = 5.3274 \text{ \AA}$ , and  $\gamma = 120^\circ$  with atomic positions of Sn at 2c (2/3, 1/3, 3/4) and H at 4e (0, 0, 0.92278) and 4f (1/3, 2/3, 0.57982), respectively. The large and small spheres represent Sn and H atoms, respectively.

1.63). In this structure, the ordered H atoms are clearly split into two categories. One sort forms semimolecular H<sub>2</sub> units (the magenta atoms in Fig. 1B) occupying hexagonal channels of the hexagonal close packing structure, whereas the other sort of H atoms occupies positions just below and above Sn atoms, forming chains Sn-H...H-Sn-H...H-Sn-H running along the c axis (Fig. 1B).

In both the *Ama2* and *P6<sub>3</sub>/mmc* phases Sn-H distances are about 1.8–1.9 Å, and Sn-Sn distances about 2.9 Å. The main differences are in the topology of the Sn framework and the relative proportion of the H<sub>2</sub> semimolecular units and monatomic hydrogen species. The transition *Ama2* → *P6<sub>3</sub>/mmc* is accompanied by a major electronic reorganization due to the appearance of monatomic hydrogen and the likely change of Sn valence. In the bond valence model the bond order is  $v_{ij} = \exp[-(R_{ij} - R_{0,ij})/b]$ , where  $R_0$  is a bond-specific parameter,  $R$  the bond length, and  $b$  a constant. Taking  $b = 0.25 \text{ \AA}$  (typical of strong covalent bonds (38)), we find that the H-H bond order in the H<sub>2</sub> semimolecular units is 0.82. Thus, hydrogen atoms in these H<sub>2</sub> units are underbonded and tend to acquire the missing electrons from the metal atoms by charge transfer. We propose to call these chemically active H<sub>2</sub> units perhydride groups; they have so far not been observed at ambient conditions, but predicted to exist at high pressures in GeH<sub>4</sub> (ref. 17) and unique lithium hydrides LiH<sub>2</sub>, LiH<sub>6</sub> and LiH<sub>8</sub> (39). Perhydride groups were also predicted in the structures of SnH<sub>4</sub> calculated in refs. 21 (*P6/mmm*) and 40 (*Cccm*), which are otherwise different from our structures. The need for charge transfer implies that perhydrides can only be formed with rather electropositive metals, such as Ge, Sn, and Li, but not Si or C. We believe that perhydrides of alkali and alkali earth metals are likely to exist and are worth exploring. Coming back to SnH<sub>4</sub> and using the estimated H-H bond order (0.82), we find that each Sn atom transfers to all four H atoms 0.72 e in the *Ama2* phase and 2.36 e in the *P6<sub>3</sub>/mmc* phase. The remaining valence is used for Sn-Sn bonds (~0.15 e per bond, and there are eight and 12 such bonds in the *Ama2* and *P6<sub>3</sub>/mmc* phases, respectively), leading us to propose the Sn(II) valence state in *Ama2* and Sn(IV) in *P6<sub>3</sub>/mmc*.

Enthalpy curves of our predicted structures as a function of pressure are presented in Fig. 2. It is noteworthy that the currently predicted structures are energetically much more favorable than the *P6/mmm* (21) and *Cccm* (40) structures. Considering the tendency to decomposition found in structure searches performed at low pressure, the enthalpy of the decomposition (Sn + 2H<sub>2</sub>, with structures of pure elements taken from refs. (41, 42) as a function of pressure) is also shown in Fig. 2. A wide

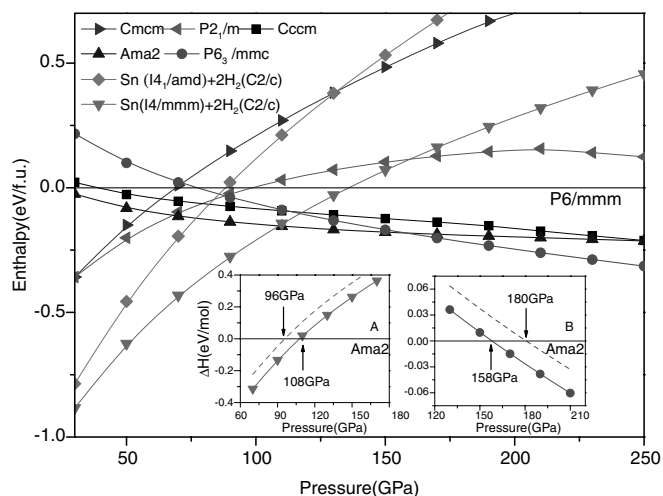


**Fig. 2.** (color online). Enthalpies per SnH<sub>4</sub> unit of various structures as a function of pressure, referenced to the *P6/mmm* phase (21). The decomposition (Sn + 2H<sub>2</sub>) enthalpies are calculated by adopting the C2/c (Ref. (41)) structure for H<sub>2</sub> and *Fd-3m*, *I4<sub>1</sub>/amd*, *I4/mmm*, and *Im-3m* (Ref. (42)) for Sn, respectively. Inset: (A) and (B) Enthalpy of decomposition (*I4/mmm*-Sn + 2C2/c-H<sub>2</sub>) and the *P6<sub>3</sub>/mmc* structure relative to the *Ama2* phase without (solid line and symbols) and with (dashed line) the zero-point motion corrections, respectively.

region of decomposition into Sn + 2H<sub>2</sub> is indeed confirmed below 108 GPa, above which *Ama2* becomes stable in the pressure of 108–158 GPa and then *P6<sub>3</sub>/mmc* structure takes over above 158 GPa. As divalent Sn(II) species are quite stable, decomposition of SnH<sub>4</sub> might also yield SnH<sub>2</sub>, the structure of which is unknown. We thus searched for the most stable high-pressure phases of SnH<sub>2</sub> at 50 and 100 GPa using the same evolutionary methodology. However, we found that SnH<sub>2</sub> + H<sub>2</sub> is 0.15 eV (0.17 eV) per SnH<sub>4</sub> unit higher in enthalpy than Sn + 2H<sub>2</sub> at 50 GPa (100 GPa). This eliminates the possibility that SnH<sub>4</sub> decomposes into SnH<sub>2</sub> + H<sub>2</sub>. One should keep in mind, however, the importance of dynamical effects stemming from the high vibrational frequencies of light hydrogen atoms, as can be seen from the phonon density of states (DOS) (Fig. 3B, D), which implies a large zero-point (ZP) energy. This has already been found to affect the relative stabilities of hydrogen and hydrides (14, 17, 41). Therefore, we estimated the ZP vibrational energies for C2/c H<sub>2</sub> (41), *I4/mmm* Sn (42), *Ama2* and *P6<sub>3</sub>/mmc* SnH<sub>4</sub> at 120 GPa using the quasi-harmonic approximation (43). It turns out that the inclusion of ZP effects does not change the topology of the phase diagram but extends the stability fields of the *Ama2* and *P6<sub>3</sub>/mmc* structures to be 96–180 GPa and above 180 GPa, respectively (insets of Fig. 2).

The calculated electronic band structures and DOS for the *Ama2* structure at 120 GPa (Fig. 3A) and *P6<sub>3</sub>/mmc* structure at 200 GPa (Fig. 3C) reveal that both phases are metallic. We found that the calculated valence bandwidths are very broad and show strong hybridization between the Sn and H orbitals. In particular, both H and Sn atoms participate in *common overlapping* bands, which is in agreement with previous theoretical prediction (12). Note that the *P6<sub>3</sub>/mmc* structure has less dispersive band structure and more bands crossing  $E_f$ , which lead to a larger electronic DOS ( $2.18 \times 10^{-2}$  states/eV/Å<sup>3</sup>) at the Fermi level  $N(E_f)$  than that ( $1.48 \times 10^{-2}$  states/eV/Å<sup>3</sup>) of the *Ama2* structure. This larger  $N(E_f)$  contributes to a higher  $T_c$ . The phonon DOS for *Ama2* SnH<sub>4</sub> at 120 GPa and *P6<sub>3</sub>/mmc* SnH<sub>4</sub> at 200 GPa are depicted in Fig. 3B, D, respectively. The absence of imaginary frequencies in the phonon DOS and phonon dispersion curves suggests that the *Ama2* and *P6<sub>3</sub>/mmc* structures are both dynamically stable. Three separate regions of phonon bands



and the two-component plasma state predicted for pure hydrogen, might also exist in these compounds.

## Materials and Methods

Ab initio evolutionary simulation for crystal structure prediction done with the Universal Structure Predictor: Evolutionary Xtallography code (27–29) searches for the structure possessing the lowest free energy at given Pressure-Temperature conditions and is capable of predicting the stable structure of a given compound for a given composition. The first generation of structures is produced randomly. Each subsequent generation is produced from 65% of the lowest-enthalpy structures of the preceding generation; in addition, the lowest-enthalpy structure always survived into the next generation. The variation operators used for producing offspring included heredity (65% structures), lattice mutation (20%), and atomic permutation (15%). The underlying structure relaxations were performed using density-functional theory (46, 47) within the Perdew-Burke-Ernzerhof (PBE) generalized gradient approximation (GGA) (48), as implemented in the Vienna Ab-initio Simulation Package code (49). The frozen core all-electron projector-augmented wave (50) method was adopted. The use of a plane-wave kinetic energy cutoff of 600 eV and dense  $k$ -point sampling were shown to give excellent convergence of the energy differences and stress tensors. EPC have been explored using the pseudopotential plane-wave method within the PBE-GGA, through the Quantum-*opEn* Source Package for Research in Electronic Structure, Simulation, and Optimization (ESPRESSO) package (51). Forces and stresses for the converged structures are optimized and checked

to be within the error between the VASP and Quantum-ESPRESSO code. Pseudopotentials for H and Sn were generated by a Troullier-Martins norm-conserving scheme (52) and tested by comparing the electronic band structures and phonon spectra with the results calculated from VASP code. In these calculations we used a kinetic energy cutoff of 50 Rydberg and a  $12 \times 12 \times 6$  Monkhorst-Pack (53)  $k$ -point grids for  $Ama2$  and  $P6_3/mmc$ , for which tests showed excellent convergence of the computed properties. The phonon spectra were calculated within density-functional perturbation theory using the Quantum-ESPRESSO package. A  $4 \times 4 \times 2$  grid of  $q$  points in the first Brillouin zone was used in the interpolation of the force constants for the phonon dispersion curve calculation. The technique for the calculation of EPC has been described in detail in our previous publication (17).

**ACKNOWLEDGMENTS.** A.B. thanks M. Martinez-Canales for discussions. G.Y.G. thanks L. J. Zhang for his help in the calculation. G.Y.G. and Y.M.M. thank China 973 Program under Grant 2005CB724400, Natural Science Allied Foundation of China under Grant 10676011, the Program for 2005 New Century Excellent Talents in University, and the 2007 Cheung Kong Scholars Program of China. G.Y.G. is also grateful to the Project 20092004 supported by Graduate Innovation Fund of Jilin University. Part of the calculation was performed with Riken SuperCombined Cluster. A.R.O. acknowledges funding from Stony Brook Research Foundation and from Intel Corp. and access to supercomputers at New York Center for Computational Sciences (U.S.A.) and Joint Supercomputer Center (Russian Academy of Sciences). A.B. acknowledges funding from the Spanish Ministry of Education (Grants BFM2003-04428 and Grant BES-2005-8057)

1. Shimizu K, Ishikawa H, Takao D, Yagi T, Amaya K (2002) Superconductivity in compressed lithium at 20 K. *Nature*, 419:597–599.
2. Struzhkin VV, Eremets MI, Gan W, Mao HK, Hemley RJ (2002) Superconductivity in dense lithium. *Science*, 298:1213–1215.
3. Deemyad S, Schilling JS (2003) Superconducting phase diagram of Li metal in nearly hydrostatic pressures up to 67 GPa. *Phys Rev Lett*, 91:167001.
4. Nagamatsu J, Nakagawa N, Muranaka T, Zenitani Y, Akimitsu J (2001) Superconductivity at 39 K in magnesium diboride. *Nature*, 410:63–64.
5. Ma Y, Tse JS, Klug DD, Ahuja R (2004) Electron-phonon coupling of  $\alpha$ -Ga boron. *Phys Rev B*, 70:214107.
6. Ashcroft NW (1968) Metallic hydrogen: A high-temperature superconductor?. *Phys Rev Lett*, 21:1748–1749.
7. Zhang L, et al. (2007) Ab initio prediction of superconductivity in molecular metallic hydrogen under high pressure. *Solid State Commun*, 141:610–614.
8. Cudazzo P, et al. (2008) Ab Initio description of high-temperature superconductivity in dense molecular hydrogen. *Phys Rev Lett*, 100:257001.
9. Loubeyre P, Occelli F, LeToullec R (2002) Optical studies of solid hydrogen to 320 GPa and evidence for black hydrogen. *Nature*, 416:613–617.
10. Goncharov AF, Gregoryanz E, Hemley RJ, Mao HK (2001) Spectroscopic studies of the vibrational and electronic properties of solid hydrogen to 285 GPa. *Proc Natl Acad Sci USA*, 98:14234–14237.
11. Narayana C, Luo H, Orloff J, Ruoff AL (1998) Solid hydrogen at 342 GPa: No evidence for an alkali metal. *Nature*, 393:46–49.
12. Ashcroft NW (2004) Hydrogen dominant metallic alloys: High temperature superconductors?. *Phys Rev Lett*, 92:187002.
13. Martinez-Canales M, et al. (2009) Novel structures and superconductivity of silane under pressure. *Phys Rev Lett*, 102:087005.
14. Kim DY, et al. (2008) Crystal structure of the pressure-induced metallic phase of  $\text{SiH}_4$  from ab initio theory. *Proc Natl Acad Sci USA*, 105:16454–16459.
15. Chen XJ, et al. (2008) Pressure-induced metallization of silane. *Proc Natl Acad Sci USA*, 105:20–23.
16. Chen XJ, et al. (2008) Superconducting behavior in compressed solid  $\text{SiH}_4$  with a layered structure. *Phys Rev Lett*, 101:077002.
17. Gao GY, et al. (2008) Superconducting high pressure phase of germane. *Phys Rev Lett*, 101:107002.
18. Eremets MI, Trojan IA, Medvedev SA, Tse JS, Yao Y (2008) Superconductivity in hydrogen dominant materials: Silane. *Science*, 319:1506–1509.
19. Degtyareva O, et al. (2007) Crystal structure of  $\text{SiH}_4$  at high pressure. *Phys Rev B*, 76:064123.
20. Li Z, Yu W, Jin CQ (2007) First-principles calculation on phase stability and metallization in  $\text{GeH}_4$  under pressure. *Solid State Commun*, 143:353–357.
21. Tse JS, Yao YS, Tanaka K (2007) Novel superconductivity in metallic  $\text{SnH}_4$  under high pressure. *Phys Rev Lett*, 98:117004.
22. Yao YS, Tse JS, Ma YM, Tanaka K (2007) Superconductivity in high-pressure  $\text{SiH}_4$ . *Europhys Lett*, 78:37003.
23. Pickard CJ, Needs RJ (2006) High-Pressure Phases of Silane. *Phys Rev Lett*, 97:045504.
24. Martinez-Canales M, Bergara A, Feng J, Grochala W (2006) Pressure induced metallization of Germane. *J Phys Chem Solids*, 67:2095–2099.
25. Feng J, et al. (2006) Structures and potential superconductivity in  $\text{SiH}_4$  at high pressure: En route to “metallic hydrogen”. *Phys Rev Lett*, 96:17006.
26. Degtyareva O, Proctor JE, Guillaume CL, Gregoryanz E, Hanfland M (2009) Formation of transition metal hydrides at high pressures. *Solid State Commun*, 149:1583–1586.
27. Oganov AR, Glass CW (2006) Crystal structure prediction using ab initio evolutionary techniques: Principles and applications. *J Chem Phys*, 124:244704.
28. Oganov AR, Glass CW, Ono S (2006) High-pressure phases of  $\text{CaCO}_3$ : Crystal structure prediction and experiment. *Earth Planet Sci Lett*, 241:95–103.
29. Glass CW, Oganov AR, Hansen N (2006) USPEX—Evolutionary crystal structure prediction. *Comput Phys Commun*, 175:713–720.
30. Ma YM, Wang YC, Oganov AR (2009) Absence of superconductivity in the high-pressure polymorph of  $\text{MgB}_2$ . *Phys Rev B*, 79:054101.
31. Oganov AR, et al. (2009) Ionic high-pressure form of elemental boron. *Nature*, 457:863.
32. Ma YM, Oganov AR, Li ZW, Xie Y, Kotakoski J (2009) Novel high pressure structures of polymeric nitrogen. *Phys Rev Lett*, 102:065501.
33. Ma YM, et al. (2009) Transparent dense sodium. *Nature*, 458:182.
34. Oganov AR, Ma YM, Glass CW, Valle M (2007) Evolutionary crystal structure prediction: Overview of the USPEX method and some of its applications. *Psi-k Newsletter*, 84:142–171.
35. Ma YM, Oganov AR, Glass CW (2007) Structure of the metallic  $\zeta$ -phase of oxygen and isosymmetric nature of the  $\epsilon$ - $\zeta$  phase transition: Ab initio simulations. *Phys Rev B*, 76:064101.
36. Li Q, et al. (2009) Superhard monoclinic polymorph of carbon. *Phys Rev Lett*, 102:175506.
37. Gaál-Nagy K, Pvone P, Strauch D (2004) ab initio study of the  $\beta$ -tin  $\rightarrow$  Imma  $\rightarrow$  sh phase transitions in silicon and germanium. *Phys Rev B*, 69:134112.
38. Urusov VS (1995) Semi-empirical groundwork of the bond-valence model. *Acta Crystallogr*, B51:641–649.
39. Zurek E, Hoffmann R, Ashcroft NW, Oganov AR, Lyakhov AO (2009) A little bit of lithium does a lot for hydrogen. *Proc Natl Acad Sci USA*, 106:17640–17643.
40. Pickard CJ, Needs RJ (2008) Structures at high pressure from random searching. *Phys Status Solidi B*, 246:536–540.
41. Pickard CJ, Needs RJ (2007) Structure of phase III of solid hydrogen. *Nat Phys*, 3:473–476.
42. Giefers H, et al. (2007) Phonon density of states of metallic Sn at high pressure. *Phys Rev Lett*, 98:245502.
43. Ma YM, Tse JS (2007) Ab initio determination of crystal lattice constants and thermal expansion for germanium isotopes. *Solid State Commun*, 143:161–165.
44. Allen PB (1972) Neutron spectroscopy of superconductors. *Phys Rev B*, 6:2577–2579.
45. Allen PB, Dynes RC (1975) Transition temperature of strong-coupled superconductors reanalyzed. *Phys Rev B*, 12:905–922.
46. Giannozzi P, Gironcoli S, Pavone P, Baroni S (1991) Ab initio calculation of phonon dispersions in semiconductors. *Phys Rev B*, 43:7231–7242.
47. Baroni S, Giannozzi P, Testa A (1987) Green's-function approach to linear response in solids. *Phys Rev B*, 58:1861–1864.
48. Perdew JP, Burke K, Ernzerhof M (1996) Generalized gradient approximation made simple. *Phys Rev Lett*, 77:3865–3868.
49. Kresse G, Furthmüller J (1996) Efficient iterative schemes for ab initio total-energy calculations using a plane-wave basis set. *Phys Rev B*, 54:11169–11186.
50. Blöchl PE (1994) Projector augmented-wave method. *Phys Rev B*, 50:17953–17979.
51. Baroni S, et al. <http://www.pwscf.org/>
52. Troullier N, Martins JL (1991) Efficient pseudopotentials for plane-wave calculations. *Phys Rev B*, 43:1993–2006.
53. Monkhorst HJ, Pack JD (1976) Special points for Brillouin-zone integrations. *Phys Rev B*, 13:5188–5192.